Mobile Robot Navigation Using a Combined Optimized Potential Field and a Boundary Following Algorithm

Samer Charifa[1], Marwan Bikdash[2]
[1]Automated Precision Inc Rockville, MD, USA
[2]Computational Science and Engineering, North Carolina A & T State University, Greensboro, NC, USA
[1]samer.charifa@apisensor.com, [2]bikdash@ncat.edu

Abstract—**We propose a novel method to the navigation of mobile robots that combines a modified potential field method with a boundary-following algorithm. The resulting method avoids many of the pitfalls of each component method, such as entrapment in local minima, oscillation in narrow corridors, hugging obstacle boundaries inefficiently, and low-quality velocity and acceleration profiles. The proposed harmonic field has non-uniform boundary conditions based on the length of the shortest path to the target computed using a graph-theoretic shortest-path solver. The boundary-following algorithm ensures the best achievable safety distance to all boundaries. The proposed method is extended to apply to rigid-body mobile robots such as line-segment robot navigating in a cluttered environment, using the concept of distributed boundary charges moving in an electrostatic potential field. The proposed method performed well, leading for instance to superior velocity and acceleration profiles.**

Keywords—Motion Planning, Harmonic Potential Field, Line-segment Robot.

I. INTRODUCTION

The artificial potential field (APF) approach is an elegant and simple method to solve path-planning as well as motion-planning problems. It yields a position-dependent feedback control, making it computationally efficient, even when the dynamics are nonlinear with multiple degrees of freedom.

APF's were introduced by Khatib [1] to yield feedback forces leading to reasonable robot paths. Connolly et al. [2] proposed a Harmonic Field with Uniform Boundary Conditions (HFUBC) obtained by solving Laplace's equation given uniform boundary conditions on the obstacle boundaries. The HFUBC proposed in [2] is mathematically proven to have no local minima in the interior of the workspace. However, the gradient of the harmonic potential function can be very high in the neighborhood of the target, and negligibly small in the rest of the workspace. As a result, the recommended feedback forces in the areas far away from the target are practically zero. Moreover, its direction cannot be computed reliably due to round-off errors introduced by the partial differential equation (PDE) solvers. Thus, the robot can practically stagnate in those areas although no local minima exist. Moreover, as a result of the unbalanced distribution of the potential values, the robot accelerates as it approaches the target and slams into it. This problem seems to be due to the perhaps-unjustifiable insistence on having a uniform field at the boundary of the obstacles.

Recently, the HFUBC has been used to solve many robotic path planning problems. Gupta et al. [3], [4] have implemented the harmonic field on internet-based navigation of a UGV. They have addressed the effect of the processing-delay when applying the harmonic field for robotic navigation over a network. Pretes et al. [5], [6] have used relaxation method to compute the harmonic field and applied their algorithm for exploration of an unknown environment. Alvarez et al. [7] implemented a harmonic field which accounts for dynamic constraints which imposed on the robot. Masoud [8], [9] has applied a harmonic-based potential field on an environment with directional constraints. He showed that the harmonic field can be modified so that it can account for directionality of the roads. More recently, Masoud [10] have extended the computation of the harmonic potential field to account for the kinematics and the dynamics of the robot by adding a nonlinear, passive damping force to the harmonic field. A drawback of applying this algorithm is oscillation in the presence of obstacles.

In this paper, we propose a harmonic potential field with optimized boundary conditions. The proposed potential field prevents several problems associated with the conventional potential field such as: oscillating in narrow corridors, vibrating in the presence of obstacles, and low level potential field values behind a shielded target. Moreover, we add a boundary following algorithm which gives the potential field more flexibility in terms of choosing the safety distance when passing through narrow corridors. Additionally, we propose a heuristic arbitration algorithm to correct the robot's orientation in order to overcome sharp corners or any similar situation.

This paper is organized as follows: In Section 2, we introduce the harmonic artificial potential field method with optimized boundary conditions. In section 3, we extend the application of the proposed potential field method to a rigid-body line-segment robot. Finally, conclusions are given in Section 4.

II. HARMONIC POTENTIAL FIELD METHOD WITH OPTIMIZED BOUNDARY CONDITIONS

A. Harmonic Field with Uniform Boundary Conditions

The HFUBC is given by the solution $\phi(r): \mathrm{R}^2 \to \mathrm{R}$ of Laplace's Equation: $\nabla^2 \phi = 0,$ with the boundary conditions:

$$\phi(r) = c_1 \text{ if } r \in \partial\beta, \text{ and } \phi(r) = c_2 < c_1 \text{ if } r \in \partial T, \quad (1)$$

where $\partial\beta$ is the union of the boundaries of all obstacles, ∂T is the target boundary, and c_1 and c_2 are constants. The force applied to the robot is then designed to be the negated gradient of the potential field, i.e. $\vec{F} = -\frac{\partial\phi}{\partial\vec{r}}$.

Figure 1 shows the model environment used throughout this paper, where the target T is the small circle to the left of the workspace and all other objects are obstacles. Figure 1 shows 100 equidistant contours of the HFUBC and illustrates the poor distribution of its values. All the contours are located inside a neighborhood around the target. This means that the potential field does not experience significant changes in its values outside the neighboring area around the target. We argue that the poor distribution of the harmonic field is due to the counterproductive choice of the uniform boundary conditions in Eq. (1).

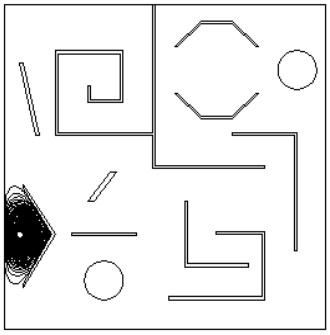

Figure 1 A hundred equidistant contour plots of the HFUBC.

B. Harmonic Field with Optimized Boundary Conditions (HFOBC)

Although the gradient lines of the HFUBC go along the correction direction to the target, the magnitude of the gradient is not accurate enough to be as a navigation method, because it does not have the necessary smooth variation [7]. This can be seen clearly in Figure 1. To solve this problem, we propose to abandon the uniformity of boundary conditions used in the HFUBC, and instead to apply $\phi(r) = \psi(r),$ whenever $r \in \partial\beta$, where $\psi(r)$ is the length of the shortest path from r to the target boundary and $\psi(r) = 0$ on the target boundary. This will result in a harmonic field with optimized boundary conditions (HFOBC). The formulation of this harmonic field can be written as:

$$\nabla^2\phi(r) = 0, \text{ and } \phi(r) = \psi(r) \text{ for } r \in \partial\beta \cup \partial T. \quad (2)$$

The boundary conditions are optimized in the sense that $\psi(r)$ represents the minimum distance to the target. These distances can be approximated using Dijkstra's algorithm on a finite-element mesh or any other spatial discretization of the configuration space such as Delaunay triangulation [11], see Figure 2. In [12], the authors developed a data structure describing a standard finite-element mesh and used this data structure to apply Dijkstra's algorithm efficiently.

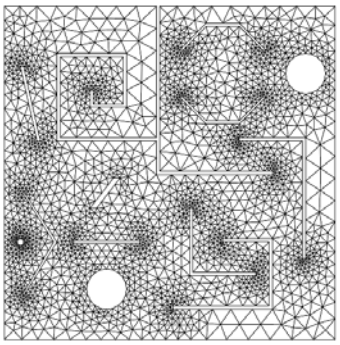

Figure 2 A typical Delaunay triangulation mesh.

Figure 3 represents the solution of Eq. (2). The equidistant-contour plots represent the values of the potential field over the workspace. Figure 4 shows the negated gradient values of the HFOBC. Clearly, the resulting field is free of local minima.

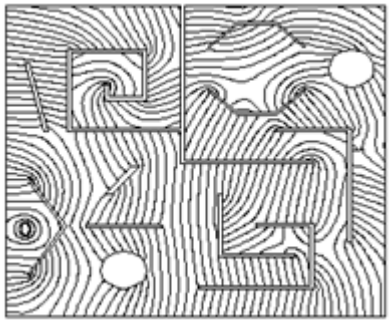

Figure 3 Contour plots of the HFOBC.

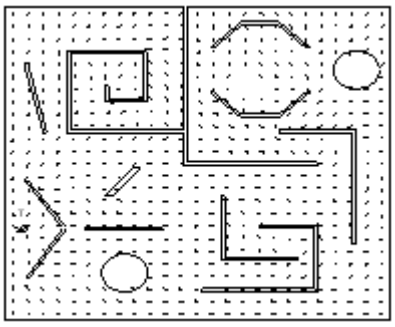

Figure 4 Gradient vectors of the HFOBC.

Theorem The HFOBC has no local minimum except on the target boundary.

Proof The HFOBC, like any harmonic function, will not have a local minimum at any internal point, as proven in [2]. Here we prove that the HFOBC has no local minimum on the boundaries of the workspace. Assume that σ and ζ are the two coordinates along two unit vectors $\vec{n}$ and $\vec{\tau}$ at some

point $r_0 \in \partial\beta$, where $\vec{\tau}$ is tangential to the boundary $\partial\beta$ and $\vec{n}$ is in the direction of the outward normal at r_0. Let $\eta(\sigma) = \psi(\sigma, 0)$ in the neighborhood of r_0, with r_0 being represented by $\sigma = 0$. Assume that $\eta(\sigma)$ has a local minimum at $\sigma = 0$. Truly, ψ cannot have a local minimum at r_0 because otherwise there will not be a path of minimum length connecting r_0 to the target. This is impossible considering the construction of . Hence, $\psi(r)$ does not have a local minimum at r_0 despite the fact that its restriction to the boundary $\eta(\sigma)$ has a minimum at r_0.

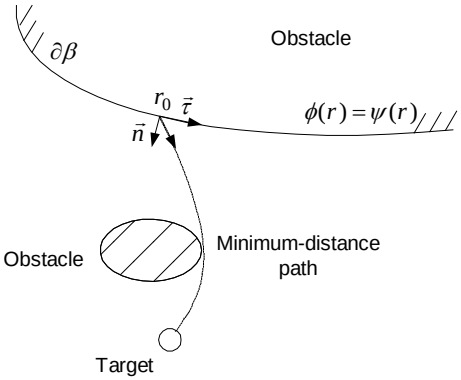

Figure 5 The HFOBC has no local minimum on an obstacle boundary.

Geometrically, $\vec{n} \cdot \vec{\nabla}\psi = c_3 < 0.$ Since both ϕ and are at least twice differentiable at any internal point, and $\phi(r) = \psi(r) \ \forall \quad r \in \partial\beta,$ then $\vec{\nabla}\psi = \vec{\nabla}\phi +$ High Order Terms (HOT) for r in the neighborhood of $r_0 \in \partial\beta.$ Then, it follows that $\vec{n} \cdot \vec{\nabla}\phi = c_3 +$ HOT $< 0.$ Hence, ϕ is local-minimum-free on the obstacle boundary.

C. Boundary Hugging Behavior of HFOBC

The HFOBC leads to a well-distributed potential field, as it is clear from the 100 equidistant contours shown in Figure 3; (compare Figure 1). A careful examination of the contours in Figure 3, as well as the many simulations of robot trajectories in Figure 6, show that the robot will often move toward the obstacle boundary and will subsequently hug that boundary while moving toward the target. As a result, the robot is expected to move on the boundary when this is advantageous (from a point of view of minimization the length of the path). An example of such a trajectory is shown by a bold line in Figure 6, where a massless robot follows one of the streamlines until it reaches the target. However, there are disadvantages, often practical, to hugging the boundary. For instance, the robot inertia may actually cause the robot to strongly collide with the boundary especially in the presence of measurement errors.

To solve this problem, we use the Boundary Following Algorithm (BFA) proposed in [13]. This BFA will keep the robot away from the obstacle within an adaptive safety distance that depends on the situation around the robot. We will later show that this improved bug-type boundary-following algorithm has excellent velocity and acceleration profiles.

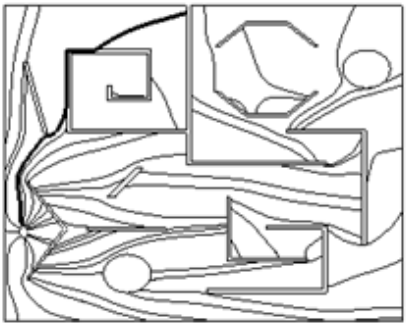

Figure 6 The streamlines of the HFOBC often follow the boundaries of the obstacles.

D. Damping Forces

We propose to add a damping/dissipative force to the robot total force in order to maintain the speed of the robot at a desirable level. The dissipative force is in the form of viscous damping $\vec{F}_b = -b\vec{v}.$ The friction coefficient b is adopted as $b = \frac{F_{\max}}{v_{sl}},$ where $F_{\max}$ is the magnitude of the maximum force that can be applied to the robot and v_{sl} is the desired speed limit. The desired speed limit depends on the robot task and on the degree of clutter. Let v_{pf} denote the speed limit in open areas, when the robot is following the potential field away from obstacle boundary. Then, we choose:

$$v_{sl} = \begin{cases} v_{pf} & \text{if robot is following the potential field,} \\ \frac{v_{pf}}{(N_w + 2N_c)} & \text{otherwise,} \end{cases}$$

where N_w is the number of walls, and N_c is the number of corners.

E. Overview of the Point-mass Navigation Algorithm

Our proposed navigation algorithm for point-mass robot can be summarized as follows:

- Use a finite-element mesh as a graph-theoretic representation of the workspace;
- Apply Dijkstra's algorithm on the mesh to approximate the shortest distances $\psi(r_i)$ from every node r_i on the boundary to the target set of boundary nodes;
- Interpolate linearly from $\psi(r_i)$ to form the boundary condition function $\psi(r)$, which gives the shortest distance from any point r on the workspace to the target;

- Solve Laplace's equation $\nabla^2\phi(r)=0,$ numerically, with the boundary conditions $\phi(r)=\psi(r)$ for $r\in\partial\beta,$ where $\partial\beta$ denotes the boundaries of the workspace;

- Navigate using the resulting potential field as long as the robot's distance L to the closest boundary is larger than a desired safety distance R;

- If $L\le R$, navigate using the boundary-following algorithm explained in [13].

III. RIGID BODY MOTION PLANNING

A. Overview

In the following, we will extend the applicability of the HFOBC algorithm to a rigid body line-segment robot, using an electrostatic analogy. The robot boundary is assumed to hold a set of fixed discrete charges interacting with the already developed potential field. The physical analogy is not pursued accurately, since the moving robot charges will create a magnetic field that will complicate the physics. These magnetic effects are assumed to be negligible in the adopted analogy. This is relevant to many applications such as moving a ladder inside a building or moving a beam in a construction site. This extension can be done by assuming that a number of fictitious charges are fixed on the robot, as can be seen in Figure 7.

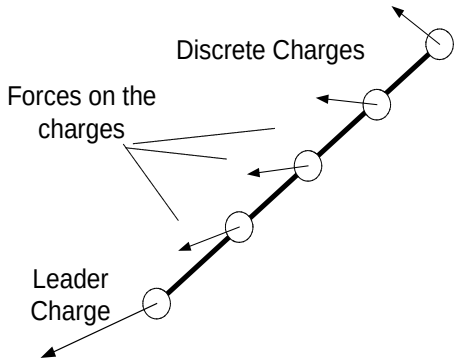

Figure 7 An example of four charges on a line-segment robot.

The HFOBC described earlier is then applied to each charge producing a distribution of forces on the robot, assumed to be a single rigid body. The force distribution must be determined by one or more actuators. New issues arise in case of rigid body navigation such as: a) Distribution of charges along the boundary of the rigid body including the possibility of dynamically reallocating the charge distribution, b) Choice of actuators, locations and constraints. These issues will be discussed below.

The algorithm of navigating a line-segment robot through a cluttered environment can be summarized as follows:

1) Use the HFOBC algorithm to compute the forces on every charge, combining the effect of the PF and the BFA (including damping and boundary layer concept [13]).

2) Apply adaptive allocation of charges.

3) Use inverse dynamics to find the actuator's forces.

B. Adaptive Allocating of Charges

The distribution of the charges on the line segment robot is important for proper navigation of the line-segment robot. If the number of charges on the segment is insufficient, collision may result between a sharp obstacle corner and a long uncharged piece of the robot. This can be avoided by choosing $d_c,$ the distance between two consecutive charges, such that: $d_c\le 2d_s,$ where d_s is the safety distance, as can be seen in Figure 8. Note that since the safety distance is adaptive, the charge separation can be adaptive as well.

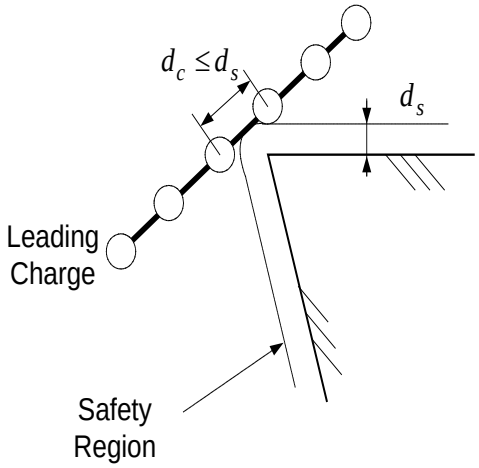

Figure 8 An example of four charges on a line-segment robot.

Since charges tend to follow the streamlines, it is desirable to assign one of the charges to be the leader charge by simply increasing its value. This will decrease the probability of the robot getting stuck and will make a long robot moves "parallel" to the streamlines.

In general the charge distribution can change in time or depending on the configuration especially in tight areas. This is achieved using an arbitration function, which changes the charges' distribution, see [14] for more detail.

C. Computing the Forces of the Actuators

The rigid body segment can be actuated in several ways. Consider the case where two omnidirectional mobile robots are placed on each end. This leads to an undetermined system of equations with 4 unknown force components and 3 constraints. A simple but suboptimal approach to solving this inverse-dynamics problem is to formulate as a quadratic minimization problem. Denote the desired resultant force by $\vec{R},$ the desired resultant torque around the Center of Gravity (CG) by $\vec{T},$ the forces of the two robots by and and two vectors from the CG to the two robots by $\vec{u},$ $\vec{v}$, as illustrated in Figure 9.

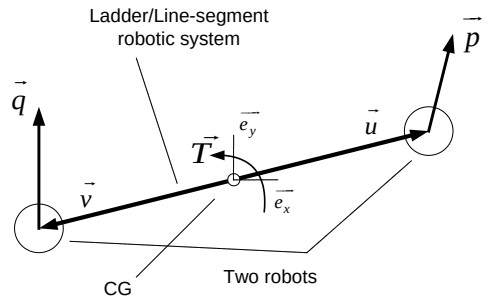

Figure 9 The distance between the charges on the line-segment robot.

A quadratic minimization problem can be set up as follows:

$$\min_{p,q} J = \|\vec{p}\|^2 + \|\vec{q}\|^2, \text{ s.t.} \quad (3)$$

$$\vec{R} = \vec{p} + \vec{q}, \quad (4)$$

$$\vec{T} = \bar{u} \times \vec{p} + \bar{v} \times \vec{q}. \quad (5)$$

Using matrix notation with $p,\ q,\ u,\ v \in \mathrm{R}^2$, the nontrivial z-component of (5) can be written as: $T_z = \vec{e}_z^{\,\mathrm{T}} \cdot \vec{T} = \bar{u}^{\mathrm{T}} \cdot p + \bar{v}^{\mathrm{T}} \cdot q,$ where $\vec{e}_z$ is a unit vector in the z direction and $\bar{u}^{\mathrm{T}} = \begin{bmatrix} -u_y & u_x \end{bmatrix}$ represents the cross product. Then, the augmented cost, using matrix notation, is:

$$L_a = \|p\|^2 + \|q\|^2 + \lambda^{\mathrm{T}}(p + q - R) + \mu\left(\bar{u}^{\mathrm{T}} p + \bar{v}^{\mathrm{T}} q - T_z\right),$$

Where $\lambda^T = \begin{bmatrix} \lambda_1 & \lambda_2 \end{bmatrix}$ and μ are the Lagrange multipliers. The solution of this minimization problem must satisfy

$$\begin{bmatrix} 2I & 0 & I & \bar{u} \\ 0 & 2I & I & \bar{v} \\ I & I & 0 & 0 \\ \bar{u}^{\mathrm{T}} & \bar{v}^{\mathrm{T}} & 0 & 0 \end{bmatrix} \begin{bmatrix} p \\ q \\ \lambda \\ \mu \end{bmatrix} = \begin{bmatrix} 0 \\ 0 \\ R \\ T \end{bmatrix}. \quad (6)$$

This solution is suboptimal in the sense that it minimized the efforts $\|\vec{p}\|$ and $\|\vec{q}\|$ but may lead to forces exceeding $F_{\max}$, the maximum allowable force on each actuator. Next, we scale down all forces until all forces are deliverable.

It should be noted that in this case we assume two robots carrying a rigid body. This can be extended to n robots cooperating to carry a rigid body of any shape.

D. Performance Evaluation

Here, we present simulation results for 3-DOF line-segment robot. Figure 10 shows the line-segment navigating in a cluttered environment using the proposed HFOBC. Note the position at which the charge allocation function switches the leader designation from one to the other to dislodge the robot when handling a tight corner. Before the switching, the leading was pulling the robot towards the target. After the switching, the leader is pushing the line-segment robot.

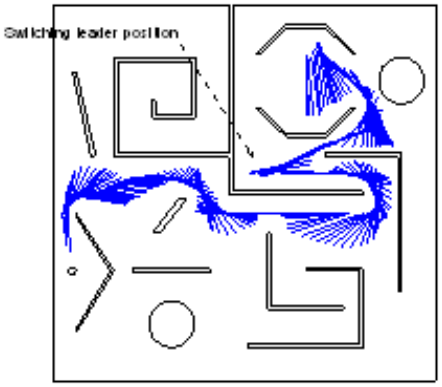

Figure 10 A line-segment robot navigating in a cluttered environment.

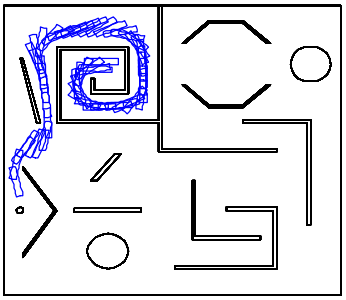

Figure 11 A rigid body moving in a cluttered environment.

Similarly, the HFOBC algorithm is simulated with a moving a rigid body in a cluttered environment using distributed charges around its circumference. The rigid body's dimensions are 10×2 ft, weights 23 Kg. In this example, two robots are used to steer this rigid body one in the front and one in the back. Each robot can deliver a maximum drag force of 600 N. The desired velocity of both robots is 5 m/sec. Figure 11 shows the rigid body navigates in the environment toward the target, very smooth obstacle avoidance, no oscillation in narrow corridors, and no stagnation points. The histories of speed of both robots are shown in Figure 12. Note that the speed values of both robots are mostly within a reasonable range of the desired speed 5±2 m/sec. In the special case when the speed experiences a spike, this happens when the rigid body motion is composed of rotation without translation. This is due to a minor limitation in the application of this algorithm; where the desired speed concept is applied only to the translation speed of the CG. Therefore, in the case of a pure rotation, the speed values at the terminals of the rotating rigid body could have higher values than the nominal desired speed. This is can be compensated for by adding one more restriction on the rotational speed.

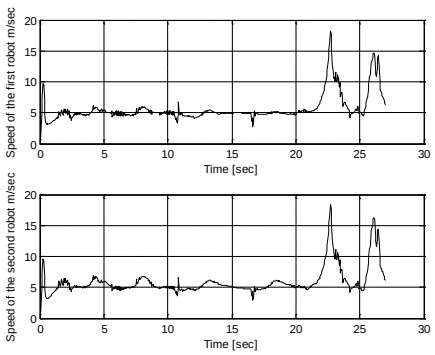

Figure 12 Histories of speed of both robots driving the rectangular rigid body.

IV. CONCLUSIONS

A new robot navigation and control algorithm has been developed and tested. It combines a new artificial harmonic potential field defined using optimized boundary conditions with a boundary-following algorithm. We proved that a point-mass robot will not experience a local minimum except at the target. The contour plots of the proposed HFOBC show that the values of the field are very well distributed over the whole workspace, in contrast to the regular harmonic field where the gradients are negligible everywhere except in the area surrounding the target. The hybrid HFOBC and BFA system was successfully extended to rigid body navigation using electrostatic energy, where charges are distributed on the boundary of the robot. The extension required several important modifications such as novel charge allocation, scaling and inverse dynamics algorithms. The results shows that the robot in all cases successfully navigate toward the target. The inverse dynamics problem has been solved for two robots carrying a rigid body from both sides. A quadratic linear optimization problem has been solved to find the forces of the actuators.

REFERENCES

[1] Khatib, Real-time obstacle avoidance for manipulators and mobile robots, International Journal of Robotics Research, 5, 90-98, 1986.

[2] C. Connolly, R. Weiss, and J. Burns, Path Planning Using Laplace's Equation, IEEE Int. Conf. Robotics and Automation, Cincinnati, OH, 2102-2106, May 1990.

[3] R. A. Gupta, A. A. Masoud, and M. Chow, A Delay-tolerant, Potential field-based, Network Implementation of an Integrated Navigation System, Int. Conf. Intelligent Robots and Systems, Beijing, China, 1121-1126, 2006.

[4] R. A. Gupta, A. A. Masoud, and M. Chow, A Network based, Delay-tolerant, Integrated Navigation System for a differential drive UGV using Harmonic Potential Field, IEEE Conference on Decision and Control, 1870-1875, San Diego, CA, 2006.

[5] E. P. Silva Jr., P. M. Engel, M. Trevisan, and M. Idiart, Exploration Method Using Harmonic Functions, Robotics and Autonomous Systems, 40, 25-42, 2002.

[6] M. Trevisan, M. Idiart, E. Prestes and P. M. Engel, Exploratory Navigation Based on Dynamical Boundary Value Problems, Journal of Intelligent and Robotic Systems, 45, 101-114, 2006.

[7] D. Alvarez, J. C. Alvarez, and R. C. Gonzalez, Online Motion Planning using Laplace Potential Fields. IEEE lnt. Conf. Robotics and Automation, Taipei, Taiwan, pp. 3347-3352, Sep. 2003.

[8] S. Masoud and A. Masoud, Constrained Motion Control Using Vector Potential Fields, IEEE Transaction Systems, Man and Cybernetic, 30, 251-272, 2000.

[9] A. Masoud and S. Masoud, Motion Planning in the Presence of Directional and Regional Avoidance Constraints Using Nonlinear, Anisotropic, Harmonic Potential Fields, IEEE Trans. Systems, Man and Cybernetic, 32, 705-723, 2002.

[10] Ahmad A. Masoud, "Kinodynamic Motion Planning: A Novel Type of Nonlinear, Passive Damping Forces and Advantages", IEEE Robotics and Automation Magazine, March 2010, pp. 85-99.

[11] O. R. Musin, Properties of the Delaunay Triangulation. Annual Symposium Computational Geometry, Nice, France, 424 - 426, June 1997.

[12] M. Bikdash, S. Karagol, and M. S. Charifa, Mesh Analysis with Applications in Reduced-Order Modeling and Collision Avoidance, COMSOL Conference, Boston, MA, 239-245, Oct. 2006.

[13] S. Charifa and M. Bikdash, Adaptive Boundary-Following Algorithm Guided by Artificial Potential Field for Robot Navigation. IEEE Workshop on Robotic Intelligence in Informationally Structured Space, Nashville, TN, 38-45, March 2009.

[14] S. Charifa, “Robotic Path Planning Using Harmonic Potential Field with Optimized Boundary Conditions”, Ph.D. Dissertation, Department of Electrical and Computer Engineering, North Carolina Agricultural and Technical State University, Greensboro, NC, USA, 2009